RSC Advances

PAPER

View Article Online
View Journal | View Issue

Cite this: *RSC Adv.*, 2022, **12**, 18559

Multiple chemical modifications and Cd^{2+} adsorption characteristics of sludge-based activated carbon

Jun Chen, *[ab] Xiaowan Dong,[a] Sisi Cao,[a] Zhaoming Chen,[a] Xiaohong Yang[a] and Jie Jin[a]

Sludge resource utilization is commonly realized through carbonization, but the use of direct carbonization to obtain sludge-based activated carbon (SAC) is not functional yet. The multiple chemical modifications were carried out to achieve N-doping and pore-making to modify SAC. The $SAC_{U-PF'}$ was synthesized by activating sludge simultaneously with uric acid and potassium ferrate. Moreover, $SAC_{N'}$, SAC_{U}, and $SAC_{PF'}$ were prepared with no additives, uric acid, and potassium ferrate, respectively. The results indicated that the different modifications affected the chemical properties and structure of SAC. The BET of $SAC_{U-PF'}$ was 56.73 m^2 g^{-1}, which was higher than that of $SAC_{N'}$ and $SAC_{PF'}$. $SAC_{U-PF'}$ possessed abundant functional groups, such as C=N and C–O. The adsorption capacity of $SAC_{U-PF'}$ for Cd^{2+} was 9.69 mg g^{-1}, 5.5 times that of $SAC_{N'}$, the adsorption process of Cd^{2+} by $SAC_{U-PF'}$ fitted well for the second-order kinetic model and Langmuir isothermal adsorption model. The XPS and chemical analysis revealed that $SAC_{U-PF'}$ and Cd^{2+} were bonded by functional groups, and the Cd^{2+} removal by $SAC_{U-PF'}$ was through complexation, anion exchange, electrostatic attraction, and pore filling. The $SAC_{U-PF'}$ was exhibited different removal capacities for different metals, Pb^{2+} and Mn^{2+} correspond to adsorption capacities of 4.9 and 8.1 mg g^{-1}. In addition, the adsorbed $SAC_{U-PF'}$ can be regenerated by sodium hydroxide. The study highlights the importance of multiple chemical modifications performed on SAC, the double coupled chemical modifications to ensure its good performance in the treatment of heavy metals in wastewater treatment.

Received 25th May 2022
Accepted 13th June 2022

DOI: 10.1039/d2ra03268f

rsc.li/rsc-advances

1. Introduction

The wastewater treatment process will produce large quantities of sludges. The current ways of sludge treatment and disposal are mainly landfill or incineration; in these processes, the resource utilization rate of sludge is low. It is well known that the sludge contains abundant organic matter, like tung wood and other materials, the characteristic suggest that sludge can be used to prepare sludge-based activated carbon (SAC). The SAC is like activated carbon, which can be used in adsorption, catalysis, and in other fields. Therefore, the technology of preparing activated carbon or carbon-based carrier from sludge has become an important alternative for future urban sludge treatment, disposal, and resource utilization.[1,2] However, SAC formed by direct carbonization of sludge is associated with some demerits such as small specific surface area, small pore volume, and poor adsorption capacity. To solve these problems, chemical modification has been widely used to change the structural characteristics of SAC and improve its application performance. Chemical treatment is an excellent approach for modifying SAC, wherein the precursor is activated with chemical reagents, and then heat treatment is performed at a relatively high temperature, which can significantly improve the structure of SAC and change the pore size distribution of SAC. This, in turn, increases the functionality of SAC. Chemical activation mainly includes acid activation (HCl, HNO_3, H_2SO_4, H_3PO_4, urea), alkali activation (NaOH, KOH, $Fe(OH)_3$), salt activation ($ZnCl_2$, $FeCl_3$), nitridation, and graphitization.[3–5] Wu[6] has utilized HCl, HNO_3, and NaOH to modify sludge. Kang[7] used KOH to activate sludge obtained from a paper mill and prepared activated carbon to adsorb heavy metals, and the results showed monolayer adsorption. Salt activation is also commonly used in the carbonization process of sludge, and the literature suggests that $ZnCl_2$ plays a major role in dehydration and vaporization, converting sludge into a high specific area SAC. Kong[8] developed a new process of pickling and pyrolysis using citric acid and $ZnCl_2$ mixed pore-forming agent to improve the performance of SAC. In the process, $ZnCl_2$ was used as the activator to obtain the maximum surface area. Studies have shown that adding pyrolusite by chemical activation method can result in a new SAC and can effectively remove heavy metal ions in wastewater.[9,10] Recently, many researchers have

[a]*School of Biology, Food and Environment, Anhui Key Laboratory of Sewage Purification and Eco-restoration Materials, Hefei University, Hefei 230601, P. R. China. E-mail: chenjun@hfuu.edu.cn; Fax: +86 551 62158406; Tel: +86 551 62158405*
[b]*Anhui Guoke Testing Technology Co., LTD, Hefei 230041, P. R. China*

shown interest in the adsorption properties of carbon-based materials. Among them, graphite-phase carbon nitride materials exhibited high chemical stability, good compatibility, more concentrated pore structure, high porosity, rich hydroxyl and carboxyl groups on the surface, and possessed great potential in the adsorption of heavy metals from wastewater.[11] For example, Yang[12] studied the removal of Cu^{2+}, and the adsorption capacity was up to 46.6 mg g^{-1}. Zhu[13] obtained carbon nitride by directly roasting melamine and adsorbing Pb^{2+} with this material. The maximum adsorption capacity exhibited by the carbon nitride material for Pb^{2+} was 7.4 mg g^{-1} in the experiment. Beygli[14] used hydroxyapatite modified carbon nitride powder to adsorb Cu^{2+}, and a striking increase in the adsorption capacity (74.5 mg g^{-1}) was observed. With the continuous acceleration of the industrial processes, many heavy metals are discharged into the environment together with industrial wastewater. Even a low concentration of heavy metals (Cd, Pb, Mn) are potentially toxic and carcinogenic, and their arbitrary discharge will seriously affect human health.[11] The adsorption method is considered to be the simplest and most effective method to remove heavy metals. Particularly, the adsorption of low-concentration heavy metals from wastewater has obvious advantages. The adsorbent, after adsorption, is also easy to recover or remove from the water medium, making it the most common water treatment method.[15] Therefore, SAC can be used as an adsorption material, and chemical modification can improve its adsorption capacity. Certain types of functional groups on the surface of SAC can effectively combine with toxic metal ions.

In the present work, two common, simple, and green activators of K_2FeO_4 and urea (CH_4N_2O) were used to change the structure of SAC. This was mainly to prepare a graphitized nitriding sludge carbon material from sludge carbon by nitrogen doping method, to improve its adsorption capacity. In this work, CH_4N_2O and K_2FeO_4 were used as chemical activators to prepare four kinds of SAC, and their properties were analyzed. The adsorption behavior of toxic metal ion Cd^{2+} was subjected to study, and the adsorption mechanism was explored by model analysis. An insight is given into the practical application of the SAC.

2. Materials and methods

2.1 Materials and reagents

The sludge was collected from the sewage treatment plant of the Hefei economic development zone. Reagents, including K_2FeO_4, CH_4N_2O, HCl (36.5%), NaOH, NaCl, $Cd(NO_3)_2$, $Pb(NO_3)_2$, $Mn(NO_3)_2$, and ethylenediamine tetraacetic acid (EDTA) were purchased from Sinopharm Chemical Reagent Co, Ltd. All chemicals were employed without further purification, and the solutions were prepared using deionized water.

2.2 Preparation of SAC

The sludge was dried at 105 °C, crushed, and then screened (80 mesh) to obtain the pretreatment sludge samples. The pretreated sludge samples were carbonized into sludge charcoal by heating at 5 °C min^{-1} to 500 °C for 120 min in an N_2 atmosphere. Then, 25 g of the so treated sludge charcoal was weighed and immersed in pure water, 250 mL of 1 mol L^{-1} $CO(NH_2)_2$ solution, 250 mL of 1 mol L^{-1} K_2FeO_4 solution, a mixture of 250 mL of 1 mol L^{-1} $CO(NH_2)_2$ and 1 mol L^{-1} K_2FeO_4, respectively, for 6 h. The samples were then dried at 80 °C, and the dried samples were heated to 800 °C at a rate of 5 °C min^{-1} under an N_2 atmosphere and maintained under the same condition for about 120 min. Then the four samples were screened through 200 mesh and soaked in 0.5 mol L^{-1} HCl for 2 h. The samples were then washed with deionized water repeatedly until neutral and dried until constant weight. The samples are denoted as $SAC_{N'}$, SAC_U, $SAC_{PF'}$, and $SAC_{U-PF'}$, respectively. A schematic diagram of preparation and reaction is represented in Fig. 1.

2.3 Characterization methods

The SAC was analyzed by scanning electron microscopy (SEM) using SU8010 cold-field emission scanning electron microscope

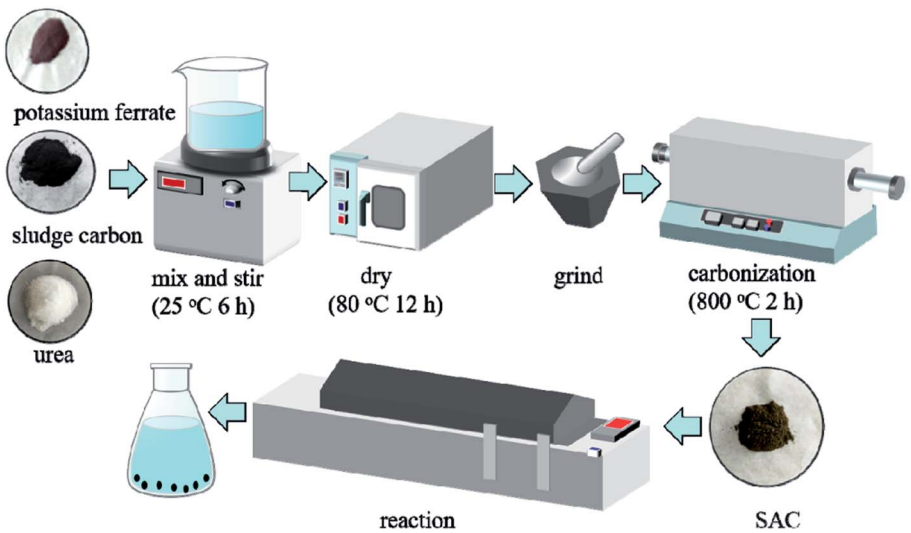

Fig. 1 Schematic diagram of preparation and reaction.

(Hitachi Company, Japan). The SAC was also analyzed by FEI-Talos-F200X (Thermo FEI, USA) transmission electron microscope (TEM). TD-3500 X-ray diffractometer (Dandong Tongda) was utilized to obtain X-ray diffraction (XRD) patterns of the SAC. The X-ray photoelectron spectroscopic (XPS) data were obtained using the Thermo Fisher K-alpha XPS instrument (Thermo Field). The SAC was scanned by using the Nicolet IS 50+ Continuum Fourier Transform Infrared Spectrometer (FTIR) (Thermo Fisher, USA). Raman spectra were obtained by the DXR laser confocal micro-Raman spectrometer (Thermo Fisher, USA). The pore size of the SAC was quantified by the nitrogen adsorption/desorption curves using a fully automated surface and porosity tester (Quantachrome, USA) and BET analysis. The zeta potential was measured by particle size and zeta analyzer (Zetasizer Nano-ZS 90, Malvern, USA). The thermogravimetric (TG) analysis used Q500 Thermo Gravimetric Analyzer (TA, USA).

2.4 Batch adsorption study

2.4.1 Adsorption property measurement. 0.1 g of each of the four different kinds of SAC samples ($SAC_{N'}$, SAC_U, $SAC_{PF'}$, and $SAC_{U-PF'}$) were added to 100 mL of Cd^{2+} solution with an initial concentration of 10 mg L^{-1}. The samples were placed in a water bath with an oscillating chamber at 25 °C and a speed of 100 r per min. During the oscillation process, samples were taken out at different times. The concentration of Cd^{2+} was measured at 228 nm using flame atomic absorption spectrometry (ZEEnit700P). The adsorption capacity and rate were calculated using eqn (1) and (2), respectively.

$$\text{Adsorption capacity: } q = V(C_0 - C_t)/m \quad (1)$$

$$\text{Adsorption rate: } R\ (\%) = \frac{(C_0 - C_t)}{C_0} \times 100\% \quad (2)$$

q (mg g^{-1}) is the adsorption capacity at that instant, V (L) is the volume of adsorbent solution, C_0 (mg L^{-1}) is the initial mass concentration of adsorbent in the solution, C_t is the mass concentration of adsorbent in the solution at the reaction time, m (g) is the mass of adsorbent, and R is the removal efficiency.

2.4.2 Research methods of adsorption kinetics. Dilute 1 g L^{-1} of Cd^{2+} reserve solution to 10 mg L^{-1} and take 100 mL of Cd^{2+} solution into a 150 mL conical flask. The solution pH will be the initial pH. Then add 0.1 g each of four kinds of SAC, and shake at 25 °C, 100 r per min at a constant temperature. The samples were measured at different time intervals (4, 8, 16, 30, 60, 90, 120, 240, 360, 480, 600, 720 min).

Pseudo-first-order model (eqn (3)), pseudo-second-order kinetic model (eqn (4)) and intra particle diffusion model (eqn (5)) were used to fit:[16]

$$\log(q_e - q_t) = \log q_e - k_1 t \quad (3)$$

$$\frac{t}{q} = \frac{1}{k_2 q_e^2} + \frac{1}{q_e} t \quad (4)$$

$$q_t = kt^{0.5} + b \quad (5)$$

where q_e (mg g^{-1}) represents the equilibrium adsorption capacity, q_t (mg g^{-1}) is the adsorption capacity at time t, k_1 (min^{-1}) and k_2 (g mg^{-1} min^{-1}) are the first-and second-order adsorption rate constants, t (min) is the time, k (mg g^{-1} $min^{-0.5}$) is the internal diffusion rate constant, and the intercept b corresponds to the boundary layer effect.

2.4.3 Adsorption isotherm study. The 100 mg L^{-1} Cd^{2+} reserve solution was successively diluted to 2.5, 5, 7.5, 10, and 12.5 mg L^{-1}, respectively. 100 mL was placed in a 150 mL conical flask, and 0.1 g of the four SAC samples were added. The oscillation box was maintained at 25 °C for 12 h at 100 r per min.

The adsorption isotherm fitting models include the Langmuir type (eqn (6)) and Freundlich type (eqn (7)), which are the commonly used isotherms to describe multilayer adsorption:[17]

$$\frac{1}{q_e} = \frac{1}{Q_m} + \frac{1}{Q_m K_L} \frac{1}{C_e} \quad (6)$$

$$\log q_e = \log K_f + \frac{1}{n} \log C_e \quad (7)$$

where q_e (mg g^{-1}) represents the equilibrium adsorption capacity, Q_m (mg g^{-1}) represents saturated adsorption capacity, C_e is the equilibrium concentration (mg L^{-1}), and K_L is the Langmuir adsorption constant. The Q_m value is proportional to the adsorption capacity. K_L represents the binding capacity to the adsorption site. $1/n$ is a constant related to adsorption, and K_f is the Freundlich adsorption constant.

2.4.4 SAC regeneration. SAC was regenerated by the solvent method, and the effects of different regenerators on the regeneration of $SAC_{U-PF'}$ were analyzed. 0.5 g of the adsorbed $SAC_{U-PF'}$ was placed in several beakers, and 0.1 mol L^{-1} of HNO_3 solution, 0.1 mol L^{-1} of NaOH solution, and 2 mmol L^{-1} of EDTA solution were configured accordingly. 50 mL of the regeneration solution was added to the beaker filled with saturated SAC for adsorption for a duration of 12 h. The regenerated SAC was washed with deionized water to neutralize. It was then dried and made to adsorb Cd^{2+} again. The process was repeated 5 times, and the results were compared.

3. Results and discussion

3.1 Characterization of SAC adsorbent

Fig. 2 shown the SEM and TEM images of four kinds of SAC samples. The surface of $SAC_{N'}$ was rough and not smooth, and the surface particles showed no obvious pore accumulation structure. In Fig. 2(b1 and b2), some lamellar or flocculent pore structures appeared in SAC_U, indicating that CH_4N_2O could modify the surface of SAC to some extent. $SAC_{PF'}$ in Fig. 2(c1) had an obvious uniform granular structure. From Fig. 2(d1) corresponding to $SAC_{U-PF'}$, it was obvious that the material surface obtained by mixing CH_4N_2O and K_2FeO_4 with nitrogen doping also had many uniform granular pore structures, and these structures tend to stack and aggregate, leading to an obvious pore structure.[4,12] Fig. 2 showed high-resolution TEM images for the four samples. After comparison, it was found

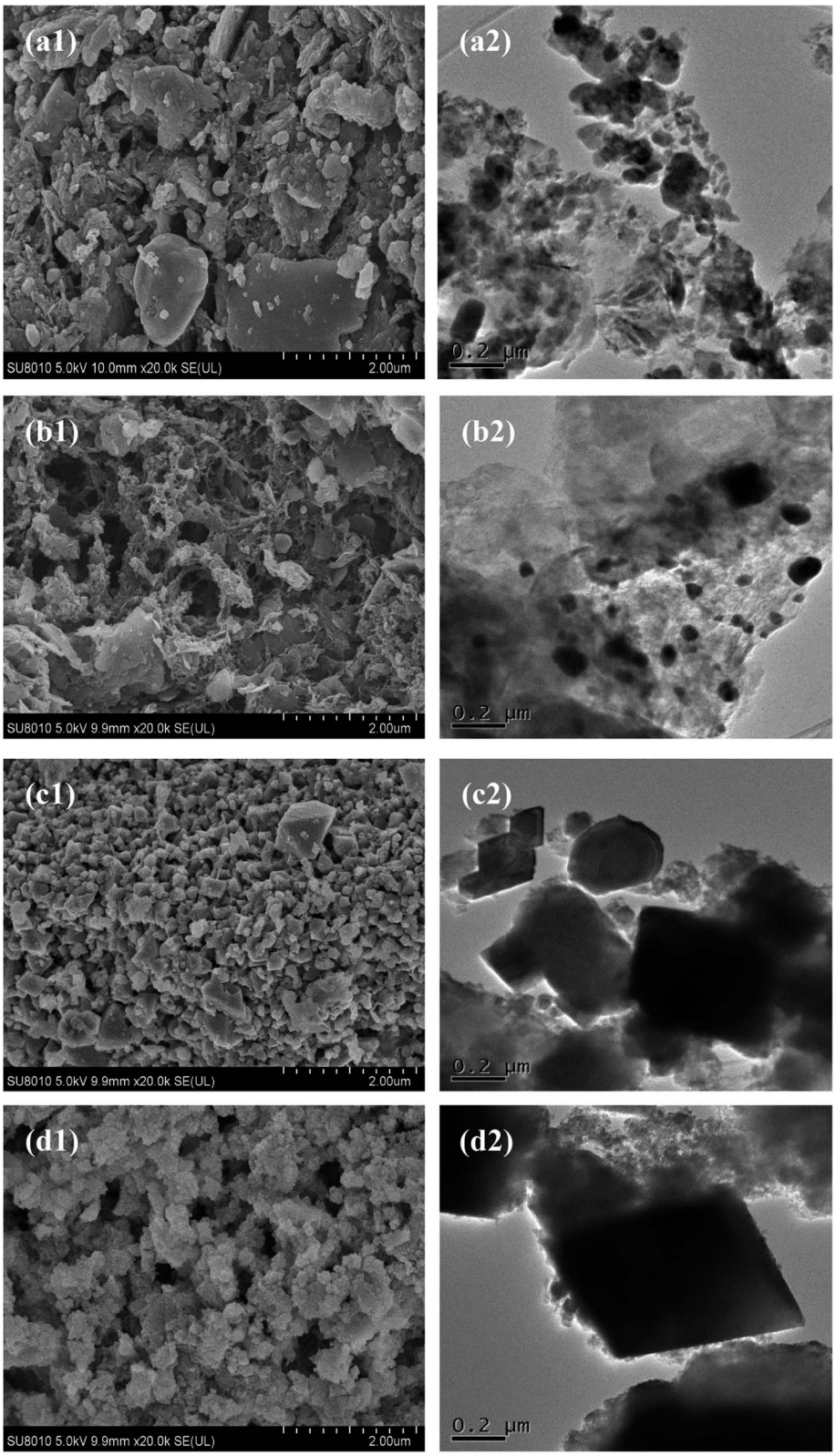

Fig. 2 SEM and TEM images of (a1 and a2) $SAC_{N'}$, (b1 and b2) SAC_{U}, (c1 and c2) $SAC_{PF'}$, and (d1 and d2) $SAC_{U-PF'}$.

that the modified SAC had obvious characteristics, the shape of $SAC_{N'}$ was irregular, the shape of SAC_{U} was fluffy, and $SAC_{PF'}$ and $SAC_{U-PF'}$ exhibited a flake square-like shape.

Fig. 3(a) shown the XRD spectra of four kinds of SAC. It can be seen from the figure that all the four SAC had diffraction peaks at $2\theta = 26.57°$, which can be considered as a 002

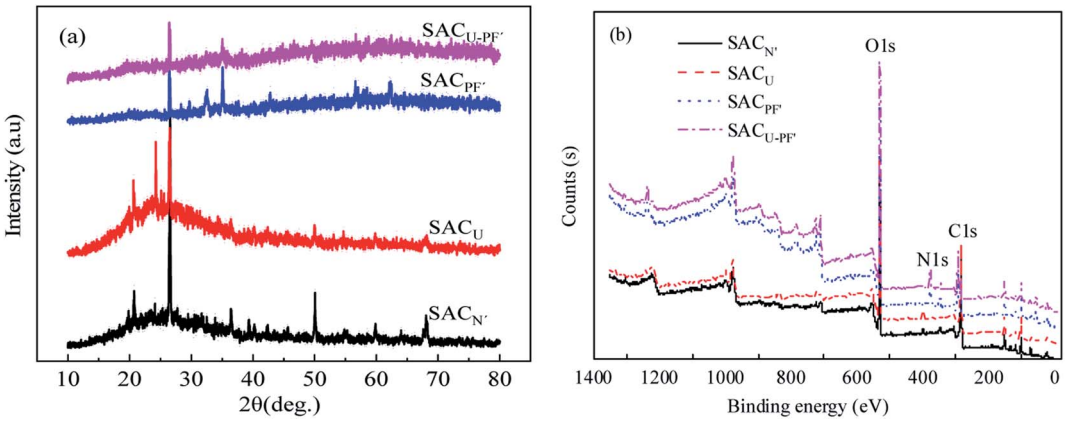

Fig. 3 (a) XRD and (b) XPS patterns of $SAC_{N'}$, SAC_U, $SAC_{PF'}$, and $SAC_{U-PF'}$.

crystalline graphite structure plane. The peak values of about $2\theta = 36°$ represent amorphous carbon. According to the comparison of JCPDS card no. (41-1487) standard card, it was found that the diffraction peak near 21° and 26° of 2θ could be related to the diffraction of quartz (SiO_2), and the signal still existed after modification. Thus suggesting that SiO_2 is the main crystalline state of SAC.[6,18] The XPS results are shown in Fig. 3(b). The peaks at 283.6 (±0.3 eV), 530.7 (±0.3 eV), and 399.7 (±0.3 eV) in the spectra, respectively, represented the binding energies of C1s, O1s, and N1s, whereas the O/C ratio of the unmodified material was increased from 0.77 to 4.65. The oxygen content in $SAC_{U-PF'}$ reached up to 73.92%, indicating that the surface of the material contains many oxygen-containing functional groups, which was consistent with the analysis of FTIR results.[19]

The FTIR of the four SAC was shown in Fig. 4(a). It can be seen from the spectrum that there were many carbon and oxygen functional groups present in the sample. The peak value at 527 cm^{-1} belonged to SiO_4^{2-} asymmetric angular motion, the peak value at 626 cm^{-1} was caused by C–O–H vibration, and the one at 777 cm^{-1} represented the stretching vibration of Si–C. 970 cm^{-1} and 1068 cm^{-1} peaks corresponded to the C–O–C stretching vibration, 1298 cm^{-1} belonged to the diffraction peak caused by C–N stretching vibration, and 1293 cm^{-1} and 1541 cm^{-1} belonged to C=C stretching vibration.[20] $SAC_{N'}$ was characterized by the antisymmetric stretching vibration of CO_3^{2-} at 1390–1510 cm^{-1}. In SAC_U, after modification by CH_4N_2O, the diffraction peak of C=N stretching vibration appeared at 1370–1610 cm^{-1}, and it possessed a carbonyl C=O stretching vibration at 1756 cm^{-1}. The peak at 2892 cm^{-1} can be ascribed to the symmetrical motion of CH_2 alkane. Similarly, the peak at 3430 cm^{-1} corresponded to O–H stretching vibration of liquid water, and 3005 cm^{-1} belonged to = C–H.[21] The strength of the O–H peak corresponding to 3688 cm^{-1} was enhanced after modification, indicating that the hydrophilic groups on the surface of SAC increased after modification.[11] Raman spectrum analysis further studied the structure of SAC, and the results are shown in Fig. 4(b). $SAC_{N'}$, SAC_U, and $SAC_{U-PF'}$ samples all exhibited a D band at 1320 cm^{-1}, which suggested the presence of defect sites or disordered sp2 hybridization related to graphitized carbon atoms and plane vibration G band (1600 cm^{-1}) of SP^2 bonded carbon atoms in a two-dimensional hexagon.[18] The degree of graphitization was directly proportional to the ratio of the intensity of D to G-band; that is, the

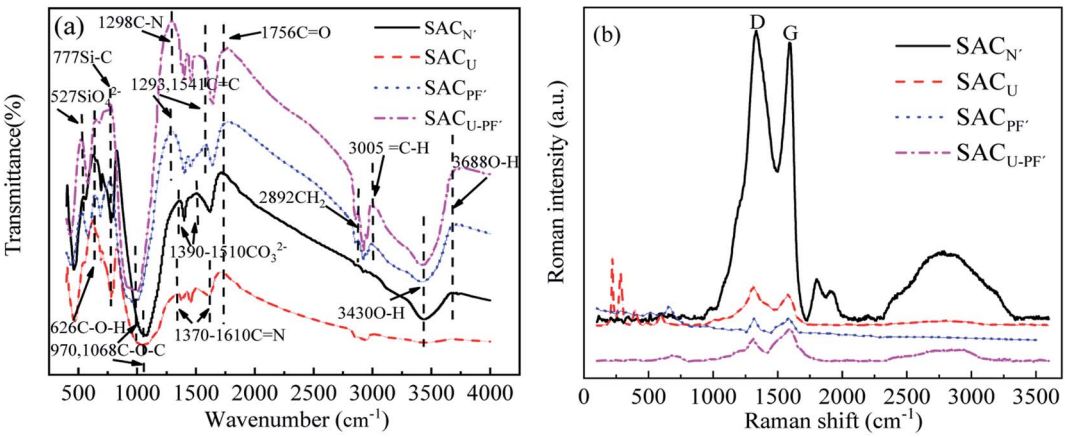

Fig. 4 (a) FTIR spectra and (b) Raman spectra of $SAC_{N'}$, SAC_U, $SAC_{PF'}$, and $SAC_{U-PF'}$.

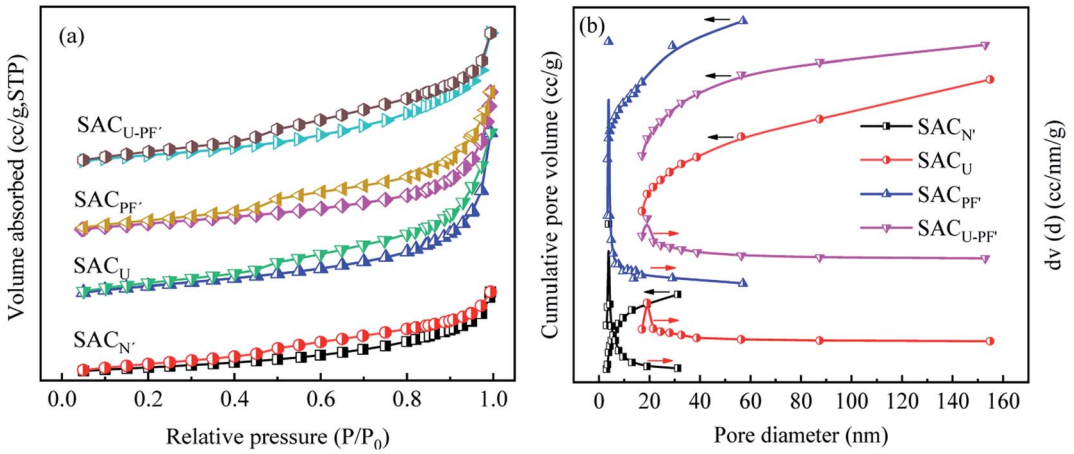

Fig. 5 (a) N_2 adsorption–desorption isotherm and (b) BJH desorption pore size distribution of $SAC_{N'}$, SAC_{U}, $SAC_{PF'}$, and $SAC_{U-PF'}$.

Table 1 BET and BJH analysis of four SAC

Adsorbents	Average pore diameter (nm)	Total pore volume ($cm^3\ g^{-1}$)	Specific surface area ($m^2\ g^{-1}$)
$SAC_{N'}$	13.42	0.7680	35.19
SAC_{U}	47.99	0.5355	69.16
$SAC_{PF'}$	21.36	0.8900	55.99
$SAC_{U-PF'}$	27.85	0.5770	56.73

higher the IG : ID ratio, the better the graphitization effect. Data from the figure suggests that IG : ID ($SAC_{U-PF'}$) > IG : ID ($SAC_{PF'}$) > IG : ID (SAC_{U}) > IG : ID ($SAC_{N'}$). The above results indicated that the mixture of CH_4N_2O and K_2FeO_4 was successfully doped with nitrogen at high temperatures, resulting in an improvement in the crystallinity of graphite carbon. The $SAC_{U-PF'}$ was prepared *via* graphitization and nitriding.[22]

The BET and BJH plots of the four SAC samples were classified as type IV according to IUPAC comparison results and were mainly mesoporous. Single-layer to multi-layer adsorption on the mesoporous wall led to slow growth of the low-pressure section. When $P/P_0 = 0.5$–0.8, the adsorption amount increased significantly, reflecting the size of the sample aperture and suggesting whether the width of the change corresponded to the size of the mesopore.[23] A hysteresis loop was observed in all materials, corresponding to the H_3 hysteresis type, which was a slit hole of flake particle accumulation consistent with the results of BJH.[18,24] The results in Fig. 5(a2–d2) and Table 1 showed that the BET and pore sizes of $SAC_{N'}$, SAC_{U}, $SAC_{PF'}$, and $SAC_{U-PF'}$ were 35.19, 69.16, 55.99, 56.73 $m^2\ g^{-1}$, and 13.42, 47.99, 21.36, 27.85 nm, respectively, moreover, all SAC were mesoporous. By comparison, it was found that the peak height of $SAC_{N'}$ was the lowest, while the other three were almost similar. This observation indicates that the number of $SAC_{N'}$ pores was small, and $SAC_{N'}$ and $SAC_{PF'}$ were microporous structures. While SAC_{U} and $SAC_{U-PF'}$ were large mesoporous structures and $SAC_{PF'}$ had the narrowest peak, indicating that the pore size was uneven.[25]

Fig. 6(a) shown the influence of pH on the zeta potential of four kinds of SAC. It can be seen from the figure that the zeta potentials of the four SAC were positive at pH = 2 and negative when pH = 6, so the pHPZC value lies between 2 to 6. At the

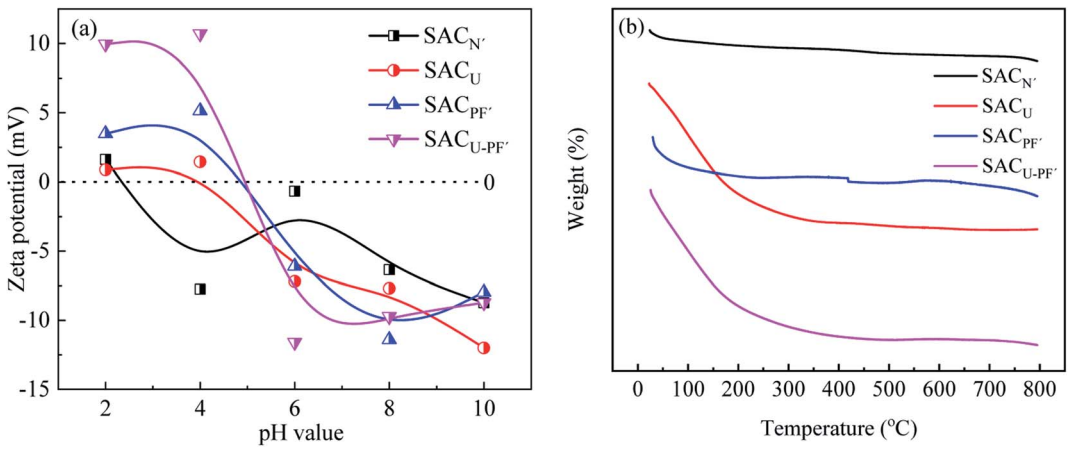

Fig. 6 (a) Zeta potential at varying pH and (b) TG of the four SAC.

respective pHPZC value, the amount of positive charge carried by the adsorbent will be equal to the amount of negative charge. This was because K_2FeO_4 contains acidic groups, while CH_4N_2O contains basic groups. As a result, after modification, the SAC exhibited weak acidity, attracted H^+, and had a positive charge, so the zeta potential value was positive. Therefore, in the subsequent single-factor experiments, when the pH was adjusted between 2 to 6, it generated electrostatic repulsion with Cd^{2+} in the solution and adsorbed Cd^{2+} by electrostatic attraction when the pH was more than 6.[26] In the Fig. 6(b), TG analysis shown that the four of SAC possessed good thermal stability, the TG variation was within 7%. As a carbon material, the decomposition of surface groups on SAC at high temperature leaded to a small amount of weight loss.

3.2 Comparison of adsorption capacities of different SAC

The comparison of the adsorption capacity of Cd^{2+} by four different SAC was demonstrated in Fig. 7.

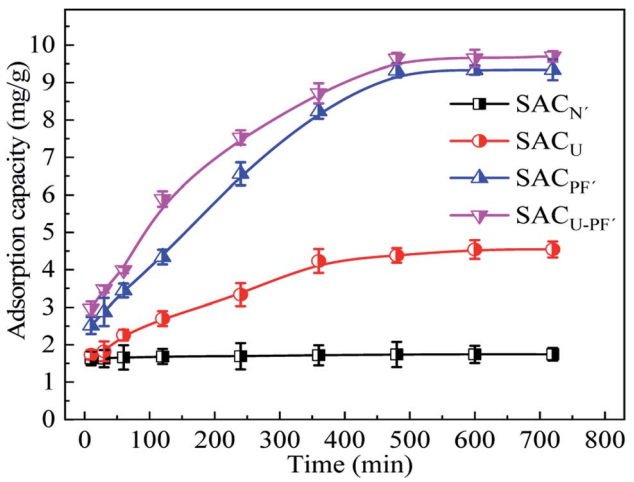

Fig. 7 Comparison of adsorption capacity of the four different SAC (Cd^{2+}: 10 mg L^{-1}; SAC: 0.1 g; pH: 6; T: 25 °C).

The results showed that K_2FeO_4 modified and K_2FeO_4 added with CH_4N_2O samples had significantly higher adsorption capacities than CH_4N_2O modified and unmodified SAC, and the maximum adsorption capacity of $SAC_{U-PF'}$ was 9.69 mg g^{-1}, which was 5.5 times than that of $SAC_{N'}$. The adsorption capacities of SAC_U and $SAC_{PF'}$ was 4.54 and 9.34 mg g^{-1}, respectively. Before 240 min, the adsorption rates of the four kinds of SAC were fast, and at about 480 min, adsorption equilibrium was attained. The rapid adsorption may be accounted to the availability of sufficient active sites, and the active sites gradually attain saturation during the process of adsorption. These results indicated that the mixed modification of K_2FeO_4 and CH_4N_2O improved the adsorption capacity of SAC. The adsorption capacity of $SAC_{U-PF'}$'s was slightly higher than $SAC_{PF'}$'s, possibly due to the further increase in the specific surface area caused by nitrogen doping.[27]

3.3 Effect of pH and temperature on SAC adsorbents

Fig. 8 demonstrated the influence of different initial pH and temperature on the adsorption of Cd^{2+} by four SAC samples.

With the increase of pH of Cd^{2+} solution from 2 to 8, the adsorption capacity of SAC also increased gradually. At a low pH value, the adsorption capacity of the material was also low because hydroxyl was not readily available, and the binding sites for adsorption of Cd^{2+} became fewer. H^+ competed with heavy metal Cd^{2+} for the active sites.[28] When the pH exceeded the initial value of 6, the adsorption capacity of $SAC_{PF'}$ and $SAC_{U-PF'}$ exhibited little difference, and the adsorption capacity of $SAC_{U-PF'}$ could reach up to 9.96 mg g^{-1}. However, when the pH of $SAC_{N'}$ and SAC_U was about 8, the adsorption capacity of $SAC_{N'}$ and SAC_U showed obvious improvement. At a higher pH, a negative charge was easily formed on the surface of the adsorbent, which generated electrostatic binding with Cd^{2+}, leading to a good adsorption efficiency. In addition to electrostatic interaction, metal ion precipitation also existed.[29] Pezoti O.[30] used the same explanation upon exploring the influence of pH on the adsorbent. Strong acid and strong base affected the

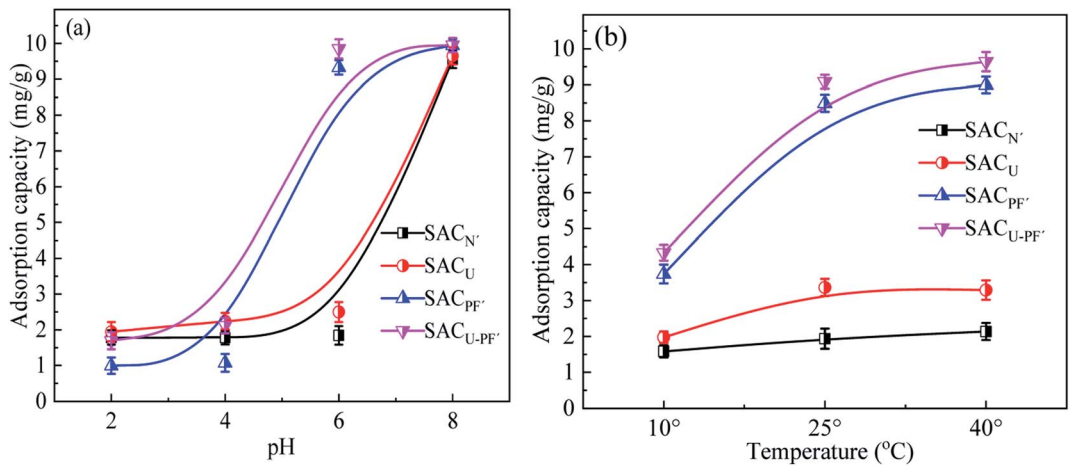

Fig. 8 The effects of (a) pH and (b) temperature on the adsorption of Cd^{2+} by the four different SAC (Cd^{2+}: 10 mg L^{-1}; SAC: 0.1 g; reaction time: 720 min).

surface charge distribution and properties of sludge-carbon material, thereby changing the electrostatic interaction between the material and Cd^{2+}, which could also be explained based on zeta potential analysis. To explore the effect of temperature on the adsorption of Cd^{2+} by SAC, three temperature gradients of 10, 25, and 40 °C were selected for the study. The results showed that temperature variation on $SAC_{N'}$ and SAC_U had little effect on the adsorption efficiency, and the adsorption effect of these two materials was poor. The temperature had a certain effect on $SAC_{PF'}$ and $SAC_{U-PF'}$. The reason may be that at low temperatures, the activation energy of solute molecules was low, and the active sites were few, which was not conducive to adsorption. As the temperature was initially increased, the active sites also increased, but when the temperature continued to rise, the active sites gradually became saturated.[31]

3.4 Adsorption kinetics

The adsorption kinetics fitting results of the adsorption model of Cd^{2+} in four different SAC are shown in Fig. 9 and 10. Table 2 presents the parameters of the kinetics model.

The comparison between Fig. 9 and Table 2 indicates that the correlation coefficient, R^2, of the second-order kinetic model was better than that of the first-order kinetic model, so it was more consistent with the adsorption process of Cd^{2+}. In addition, the correlation coefficient of $SAC_{U-PF'}$ was the highest ($R^2 = 0.996$), and the calculated equilibrium adsorption value (q_e) of $SAC_{U-PF'}$ using second-order kinetic simulation was 8.767, which showed the least deviation from the experimental value of 9.69. Therefore, based on the above analysis, the adsorption behavior of $SAC_{U-PF'}$ for Cd^{2+} was more apt to be fitted with the second-order kinetic model, mainly relying on electrostatic attraction for adsorption.[32] As can be seen from Fig. 10, $SAC_{U-PF'}$ particle diffusion model in the fitting curve is divided into two sections. The first stage was mainly for the spread of microporous adsorption and diffusion of ions in the solution to the active sites on the surface of the adsorbent. The second stage ions continue to be diffused into microporous and mesoporous channels, with higher rates for $SAC_{PF'}$ and $SAC_{U-PF'}$ in the second stage, indicating the dominance of mesoporous adsorption.[33]

3.5 Adsorption isotherms

The fitting results of Langmuir type and Freundlich type adsorption thermodynamics are demonstrated in Fig. 11 and Table 3.

According to the fitting results, the Langmuir isotherm model was quite consistent with the adsorption process of Cd^{2+}, which is evident from the data given in Table 3. The correlation coefficient R^2 of the Langmuir was higher than that of the

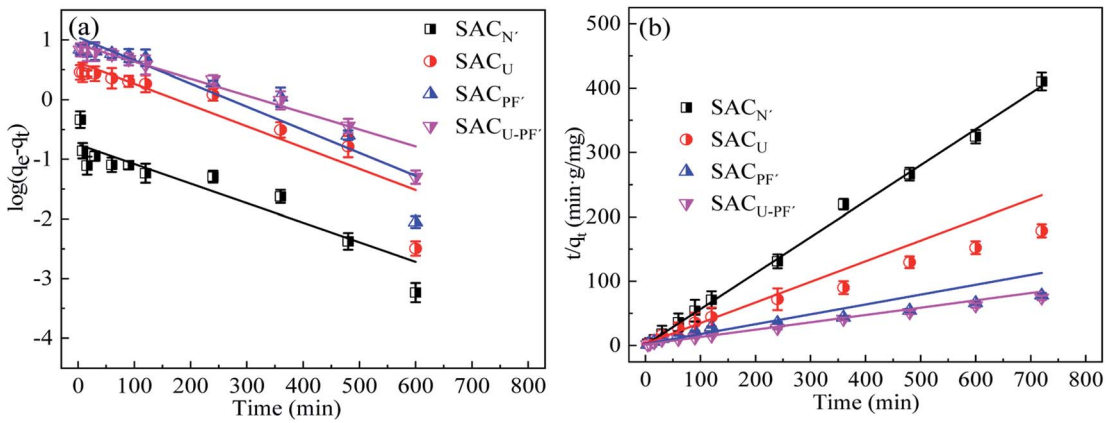

Fig. 9 (a) Pseudo-first order and (b) pseudo-second order kinetic model of Cd^{2+} adsorption by the four SAC (Cd^{2+}: 10 mg L^{-1}; SAC: 0.1 g; pH: 6; T: 25 °C; reaction time: 720 min).

Table 2 The kinetic parameters and intra-particle diffusion parameters of four SAC

	First-order kinetic model			Second-order kinetic model			Intra particle diffusion parameters	
Adsorbents	q_e (mg g^{-1})	k_1 (min^{-1})	R^2	q_e (mg g^{-1})	k_2 (g mg^{-1} min^{-1})	R^2	$K_{P_1}K_{P_2}$ (mg·(g $min^{1/2}$)$^{-1}$)	$R_1^2R_2^2$
$SAC_{N'}$	0.187	0.008	0.879	1.789	0.395	0.984	0.014	0.047
							0.005	0.969
SAC_U	4.209	0.008	0.839	4.231	0.019	0.869	0.115	0.963
							0.125	0.934
$SAC_{PF'}$	11.061	0.009	0.868	8.521	0.006	0.955	0.206	0.97
							0.343	0.843
$SAC_{U-PF'}$	8.698	0.007	0.953	8.767	0.007	0.996	0.248	0.969
							0.288	0.891

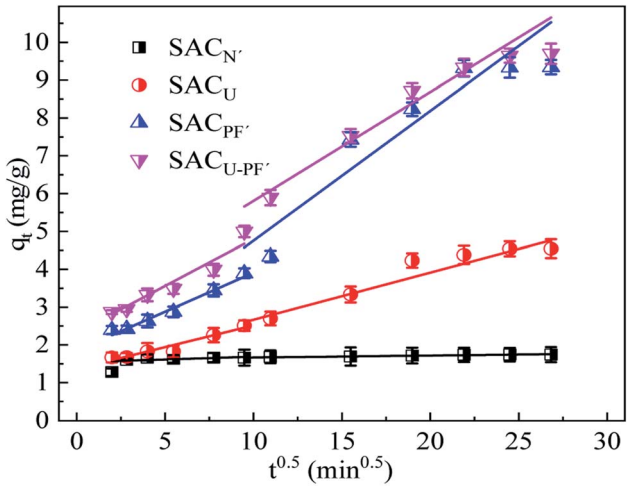

Fig. 10 Intra-particle diffusion model of Cd^{2+} adsorption by the four SAC (Cd^{2+}: 10 mg L^{-1}; SAC: 0.1 g; pH: 6; T: 25 °C; reaction time: 720 min).

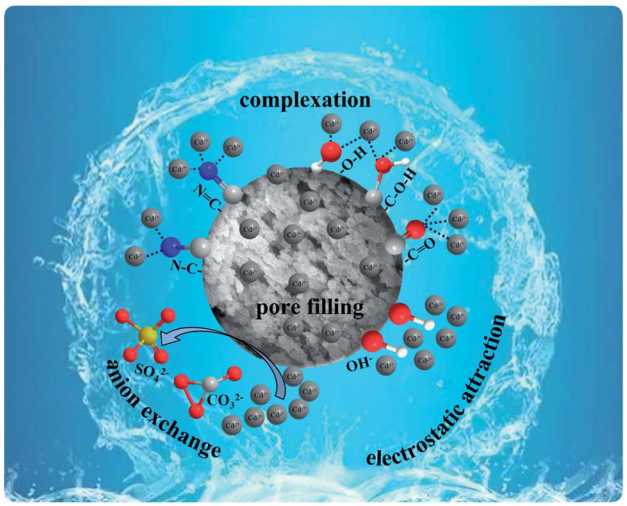

Fig. 12 Mechanism diagram of adsorption of Cd^{2+} by SAC$_{U-PF'}$.

Freundlich, and monomolecular adsorption was the main adsorption behavior.[34,35] The fitting of the Freundlich isotherm model was poor, possibly due to the limited active sites on the surface of graphitized nitride sludge carbon material.[36,37]

3.6 Adsorption mechanism

According to the structural characteristics and adsorption performance of SAC, the mechanism of adsorption of Cd^{2+} by SAC was conjectured and displayed in Fig. 12. The adsorption mechanism mainly included pore filling, complexation, electrostatic attraction, and anion exchange. As a typical carbon structure, SAC had many pores in which Cd^{2+} could accumulate by pore filling. The heavy metal, Cd^{2+}, and SAC adsorbent surface develop an electrostatic attraction. Due to the electrostatic attraction, metal ions are gathered on the SAC surface by the displacement of other ions, ion exchange, ion accumulation on the surface of the adsorbent, and physical adsorption. The metal ions and the material itself involves in

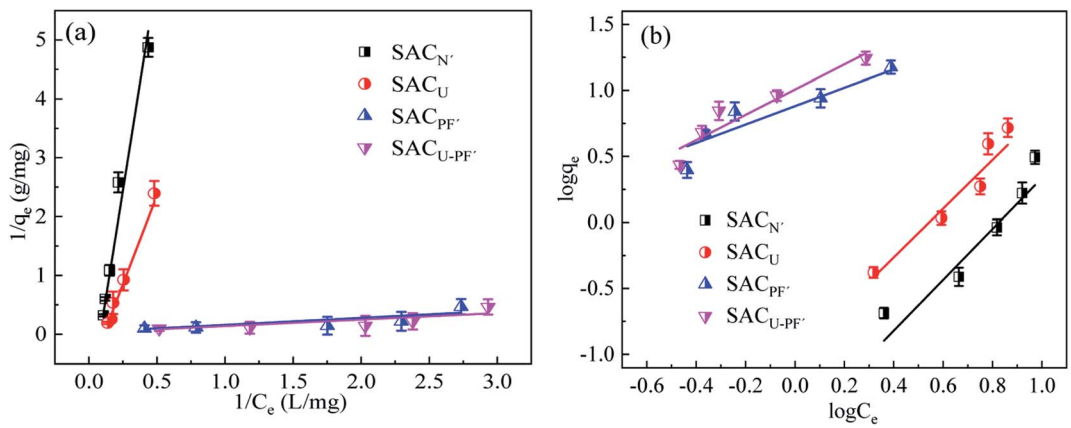

Fig. 11 (a) Langmuir and (b) Freundlich isotherm model of Cd^{2+} adsorption by the four SAC (SAC: 0.1 g; pH: 6; T: 25 °C; reaction time: 720 min).

Table 3 Freundlich and Langmuir adsorption isotherm simulation parameters of four SAC

	Langmuir			Freundlich		
Adsorbents	Q_m (mg g^{-1})	k_L (L mg^{-1})	R^2	n	k_f (mg g^{-1}(mg L^{-1})$^{-1/n}$)	R^2
SAC$_{N'}$	0.834	0.082	0.95	0.519	0.026	0.832
SAC$_{U}$	1.531	0.109	0.932	0.542	0.099	0.881
SAC$_{PF'}$	23.88	0.35	0.876	1.436	7.6	0.875
SAC$_{U-PF'}$	23.3	0.389	0.954	1.046	10.144	0.863

complexation with oxygen-containing functional groups. The XPS spectra before and after adsorption were analyzed, and the results are demonstrated in Fig. 13(a). After adsorbing Cd^{2+} onto SAC, the characteristic peak of C–O exhibited a redshift, indicating the loss of electrons by C and O and consequently gain of electrons by Cd. According to the hybrid orbital theory, it may be observed in Fig. 13(b) that the lone pair of electrons from N $2s^2p^3$, O $2s^2p^4$, and hybrid orbital could occupy the Cd $5s^2d^{10}$ orbital, and a strong force can be established between active groups (C–O, C–N) and the metal ion (Cd^{2+}). This suggests that a coordinate bond (Cd–C, Cd–O, and Cd–N) could be validated between Cd^{2+} and the active group on the surface of SAC.[38] According to the analysis of FTIR results, the surface of the adsorbent contained some anions, such as SO_4^{2-} and CO_3^{2-}, which could exchange ions with Cd^{2+}.[39] Similarly, the hydroxyl, carbonyl, and aldehyde groups on the surface of the adsorbent reacted with Cd^{2+}. The result had also been confirmed by other studies, and the hydroxyl group in the adsorbent was responsible for the adsorption of heavy metals.[40] In addition, according to the

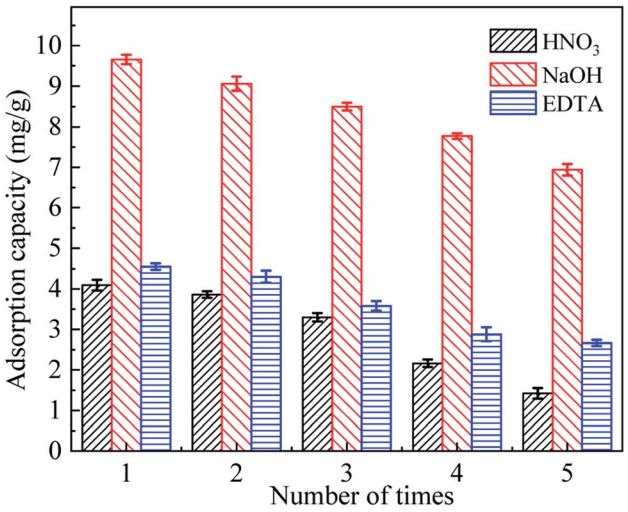

Fig. 14 Regeneration effect of three different regenerators on Cd^{2+} adsorption by $SAC_{U-PF'}$ (Cd^{2+}: 10 mg L^{-1}; $SAC_{U-PF'}$: 0.1 g; pH: 6; T: 25 °C; reaction time: 720 min).

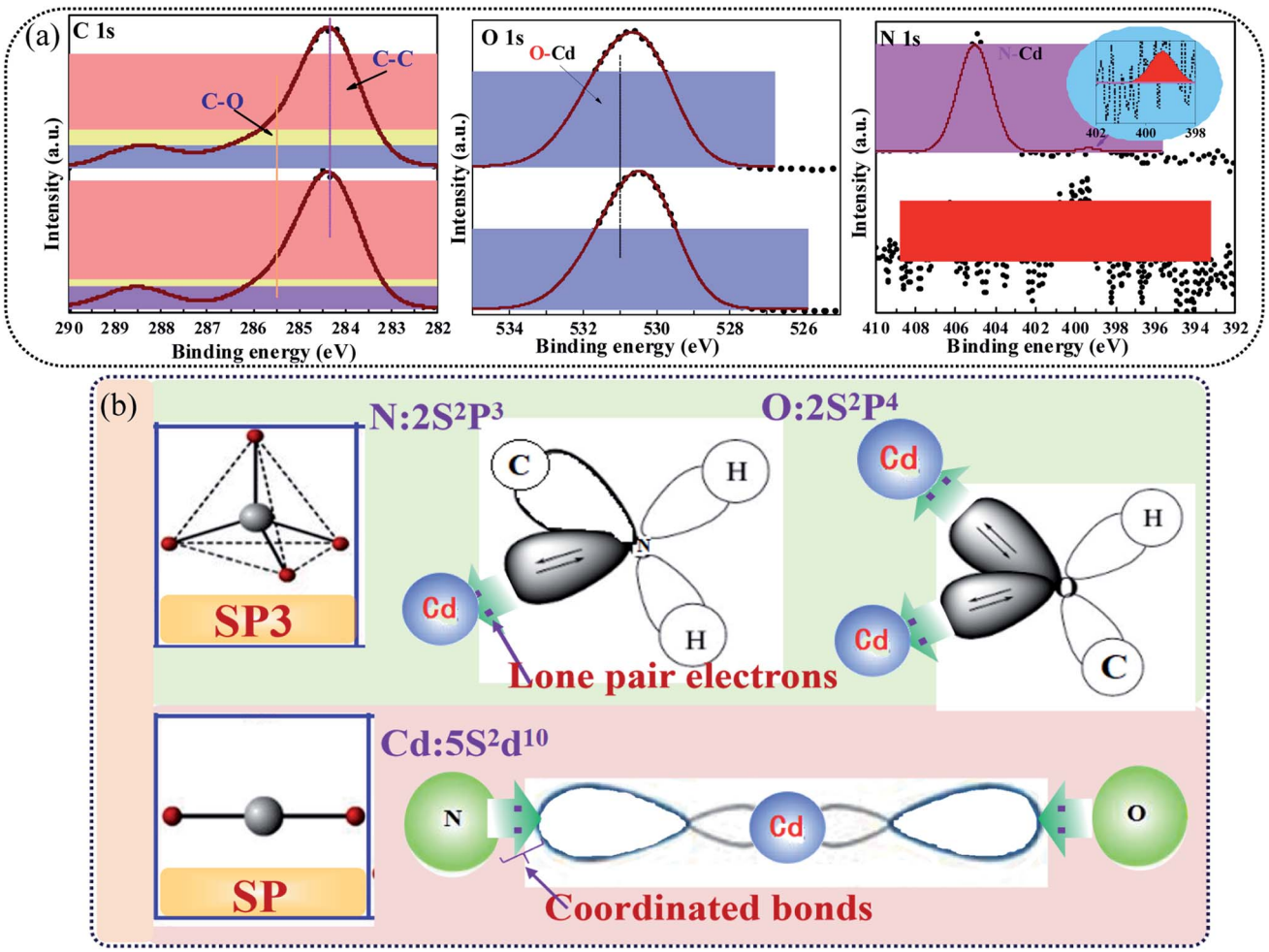

Fig. 13 Schematic illustration of (a) XPS spectra and (b) chemical bonding of Cd^{2+} by $SAC_{U-PF'}$.

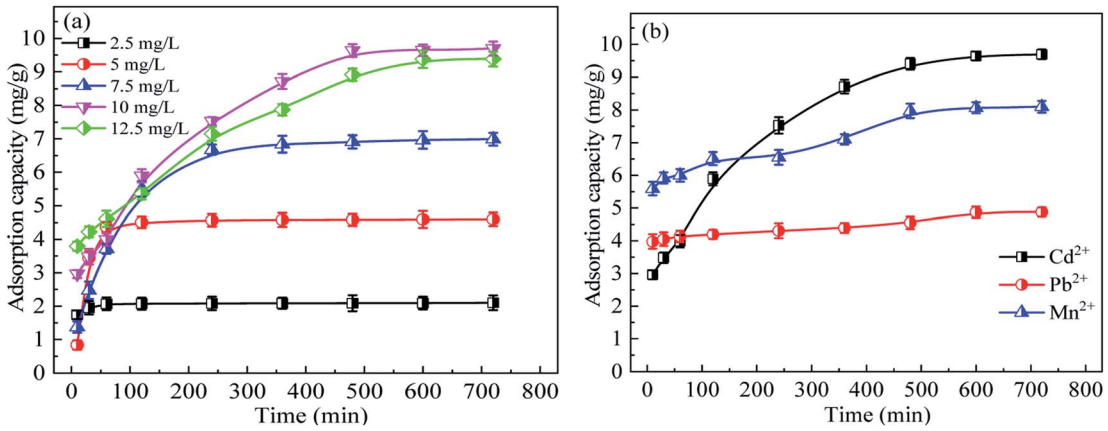

Fig. 15 (a) Adsorption of different initial concentration of Cd^{2+} and (b) different heavy metal ions by $SAC_{U-PF'}$ (concentration of heavy metal ions: 10 mg L^{-1}; $SAC_{U-PF'}$: 0.1 g; pH: 6; T: 25 °C).

zeta potential, when pH < pHpzc, the adsorbent will have a more positive charge, leading to competition between Cd^{2+} and the adsorbent. When pH was higher, the adsorbent functional group will possess a negative charge, resulting in electrostatic attraction with Cd^{2+}, thereby affecting the removal effect.[41]

3.7 SAC adsorbent regeneration

Strong acids, bases, and surfactants could regenerate metal sorbents.[42] The analytical regeneration of $SAC_{U-PF'}$ with three different regenerating agents (HNO_3, NaOH, and EDTA) and the readsorption of Cd^{2+} were subjected to study. The adsorption effect is illustrated in Fig. 14.

As shown in Fig. 14, NaOH showed the best regeneration effect, and the adsorption capacity after five cycles reached 7.37 mg g^{-1}, while EDTA showed the second-best effect, which may be related to the positive charge on the Cd^{2+} ion.[43] After successive regeneration, the adsorption efficiency also gradually decreased, which may be due to incomplete desorption and ablative. It was worth noting that the performance of $SAC_{U-PF'}$ was even damaged to a certain extent.[44] NaOH exhibited a good regeneration effect and could be used as a regenerating agent for recovering $SAC_{U-PF'}$ adsorbed with heavy metal ions. This result provided some theoretical support for subsequent studies on the regeneration of metal sorbents.

3.8 Application test of SAC

The application test of $SAC_{U-PF'}$ for low-concentration heavy metal removal from wastewater was performed. $SAC_{U-PF'}$ was employed to test different concentrations and types of metal ions, as displayed in Fig. 15.

The adsorption effect of $SAC_{U-PF'}$ at different Cd^{2+} concentrations was shown in Fig. 15(a), from which it was evident that the adsorption amount increased with increasing the concentration, but when the concentration of Cd^{2+} exceeded 10 mg g^{-1}, the adsorption effect decreased. Moreover, the adsorption amount at the concentration of 12.5 mg g^{-1} was lower than that at 10 mg g^{-1}. Adsorption eventually became difficult and tended to equilibrate over time.[11] Therefore, the SAC possesses a certain application value for low concentration metal removal from wastewater. Fig. 15(b) shows the adsorption effect of $SAC_{U-PF'}$ on Cd^{2+}, Mn^{2+}, and Pb^{2+}. The adsorption capacity of Pb^{2+} was only 4.88 mg g^{-1}, Mn^{2+} was 8.1 mg g^{-1}, and Cd^{2+} was the best, 9.69 mg g^{-1}. In addition, over time, the adsorption of Pb^{2+} and Mn^{2+} gradually slowed down, while the adsorption rate of Cd^{2+} was fast in the early stage and gradually flattened out later, which may be due to the presence of many adsorption sites in the early stage. As the adsorption progressed, the availability of adsorption sites decreased, and the adsorption became more and more difficult. It can be concluded that the $SAC_{U-PF'}$ can be used to adsorb other low concentrations of heavy metal from wastewater as well.

4. Conclusions

$SAC_{U-PF'}$ was prepared by multiple chemical modifications employing K_2FeO_4 and CH_4N_2O. Such modifications were executed based on the fact that suitable chemical activators could promote the characteristics of the $SAC_{U-PF'}$ by generating abundant pores with variable sizes and functional groups, which in turn was beneficial to the adsorption of Cd^{2+}. The maximum adsorption capacity of $SAC_{U-PF'}$ was 9.69 mg g^{-1}, 5.5 times that of $SAC_{N'}$. The $SAC_{U-PF'}$ adsorbent can be used in the removal of low concentrations of heavy metals from wastewater. The approach of multiple chemical modifications improved the adsorption performance of heavy metals in wastewater and increased the possibility of sludge resource utilization.

Conflicts of interest

There are no conflicts to declare.

Acknowledgements

This research was supported by the National Key R&D Program of China (2020YFC1908601, 2020YFC1908602). Science Development Fund Project of Hefei University (22040521004).

References

1 K. Smith, G. Fowler, S. Pullket, *et al.*, Sewage sludge-based adsorbents: A review of their production, properties and use in water treatment applications, *Water Res.*, 2009, **43**, 2569–2594.

2 Y. Xiao, A. Raheem, L. Ding, *et al.*, Pretreatment, modification and applications of sewage sludge-derived biochar for resource recovery-A review, *Chemosphere*, 2022, **287**, 131969.

3 A. Ros, M. A. Lillo-Rodenas, E. Fuente, *et al.*, High surface area materials prepared from sewage sludge-based precursors, *Chemosphere*, 2006, **65**(1), 132–140.

4 B. Yan, L. H. Zhang, W. Jiang, *et al.*, Research progress on producing sludge activated carbon doped with Ce, *Prog. Environ. Sci. Eng.*, 2013, **610–613**, 1565.

5 D. Zhang, R. Hou, W. Wang, *et al.*, Recovery and reuse of floc sludge for high-performance capacitors, *Front. Environ. Sci. Eng.*, 2022, **16**(6), 1–12.

6 X. Chun, L. Wu, H. Li, *et al.*, Effects of chemical modification on physicochemical properties and adsorption behavior of sludge-based activated carbon, *J. Environ. Sci.*, 2021, **100**(02), 342–354.

7 H. Y. Kang, S. S. Park and Y. S. Rim, Preparation of activated carbon from paper mill sludge by KOH-activation, *Korean J. Chem. Eng.*, 2006, **23**(6), 948–953.

8 L. J. Kong, Y. Xiong, S. H. Tian, *et al.*, Preparation and characterization of a hierarchical porous char from sewage sludge with superior adsorption capacity for toluene by a new two-step pore-fabricating process, *Bioresour. Technol.*, 2013, **146**, 457–462.

9 R. Z. Xie, W. J. Jiang, L. Wang, *et al.*, Effect of pyrolusite loading on sewage sludge-based activated carbon in Cu(II), Pb(II), and Cd(II) adsorption, *Environ. Prog. Sustainable Energy*, 2014, **32**(4), 1066–1073.

10 L. Wang, Y. Chen, W. J. Jiang, *et al.*, Removal of Cu^{2+} from aqueous solution using sewage sludge-based activated carbons with pyrolusite modification, *Environ. Sci. Technol.*, 2011, **34**(11), 118–122.

11 M. Anbia and M. Haqshenas, Adsorption studies of Pb(II) and Cu(II) ions on mesoporous carbon nitride functionalized with melamine-based dendrimer amine. Iit, *J. Environ. Sci. Technol.*, 2015, **12**(8), 2649–2664.

12 S. T. Yang, Y. L. Chang, H. F. Wang, *et al.*, Folding/aggregation of graphene oxide and its application in Cu^{2+} removal, *J. Colloid Interface Sci.*, 2010, **351**(1), 122–127.

13 L. Zhu, L. J. You, Y. Wang, *et al.*, The application of graphitic carbon nitride for the adsorption of Pb^{2+} ion from aqueous solution, *Mater. Res. Express*, 2017, **4**(7), 075606.

14 R. A. Beygli, N. Mohaghegh and E. Rahimi, Metal ion adsorption from wastewater by g-C_3N_4 modified with hydroxyapatite: a case study from Sarcheshmeh acid mine drainage, *Res. Chem. Intermed.*, 2019, **45**(4), 2255–2268.

15 A. Yazdankhah, S. E. Moradi, S. Amirmahmoodi, *et al.*, Enhanced sorption of cadmium ion on highly ordered nanoporous carbon by using different surfactant modification, *Microporous Mesoporous Mater.*, 2010, **133**(1–3), 45–53.

16 J. P. Simonin, On the comparison of pseudo-first order and pseudo-second order rate laws in the modeling of adsorption kinetics, *Chem. Eng. J.*, 2016, **300**, 254–263.

17 S. Banerjee, S. Mukherjee, A. LaminKa-ot, *et al.*, Biosorptive uptake of Fe^{2+}, Cu^{2+} and As^{5+} by activated biochar derived from Colocasia esculenta: Isotherm, kinetics, thermodynamics and cost estimation, *J. Adv. Res.*, 2016, **7**(5), 597–610.

18 L. Sun, Y. Fu, C. G. Tian, *et al.*, Isolated boron and nitrogen sites on porous graphitic carbon synthesized from nitrogen-containing chitosan for supercapacitors, *Chemsuschem*, 2014, **7**(6), 1637–1646.

19 O. Duman, C. O. Diker and S. Tunc, Development of highly hydrophobic and superoleophilic fluoro organothiol-coated carbonized melamine sponge/rGO composite absorbent material for the efficient and selective absorption of oily substances from aqueous environments, *J. Environ. Chem. Eng.*, 2021, **9**(2), 105093.

20 A. F. M. Streit, L. N. Cortes, S. P. Druzian, *et al.*, Development of high quality activated carbon from biological sludge and its application for dyes removal from aqueous solutions, *Sci. Total Environ.*, 2019, **660**, 277–287.

21 K. B. Yang, J. H. Peng, C. Srunivasakannan, *et al.*, Preparation of high surface area activated carbon from coconut shells using microwave heating, *Bioresour. Technol.*, 2010, **101**(15), 6163–6169.

22 Y. N. Gong, D. L. Li, C. Z. Luo, *et al.*, Highly porous graphitic biomass carbon as advanced electrode materials for supercapacitors, *Green Chem.*, 2017, **19**(17), 4132–4140.

23 M. Thommes, K. Kaneko, A. V. Neimark, *et al.*, Physisorption of gases, with special reference to the evaluation of surface area and pore size distribution (IUPAC Technical Report), *Pure Appl. Chem.*, 2015, **87**(9–10), 1051–1069.

24 L. Qi, T. Xu, Z. Wang, *et al.*, Pore characterization of different types of coal from coal and gas outburst disaster sites using low temperature nitrogen adsorption approach, *Int. J. Min. Sci. Technol.*, 2017, **27**(2), 371–377.

25 L. Yang, Y. Zhan, Y. Gong, *et al.*, Development of eco-friendly CO_2-responsive cellulose nanofibril aerogels as "green" adsorbents for anionic dyes removal, *J. Hazard. Mater.*, 2021, **405**, 124194.

26 Y. Li, S. M. Zhu, Q. L. Liu, *et al.*, N-doped porous carbon with magnetic particles formed in situ for enhanced Cr (VI) removal, *Water Res.*, 2013, **47**(12), 4188–4197.

27 T. T. Song, W. J. Tian, K. L. Qiao, *et al.*, Adsorption behaviors of polycyclic aromatic hydrocarbons and oxygen derivatives in wastewater on N-doped reduced graphene oxide, *Sep. Purif. Technol.*, 2020, **254**, 117565.

28 M. Zhang, Y. Zhang and R. Helleur, Selective adsorption of Ag+ by ion-imprinted O-carboxymethyl chitosan beads grafted with thiourea-glutaraldehyde, *Chem. Eng. J.*, 2015, **264**, 56–65.

29 L. S. Hu, C. Y. Guang, Y. Liu, *et al.*, Adsorption behavior of dyes from an aqueous solution onto composite magnetic lignin adsorbent, *Chemosphere*, 2020, **246**, 125757.

30 O. Pezoti, A. L. Cazetta, K. C. Bedin, *et al.*, NaOH-activated carbon of high surface area produced from guava seeds as a high-efficiency adsorbent for amoxicillin removal: Kinetic, isotherm and thermodynamic studies, *Chem. Eng. J.*, 2016, **288**, 778–788.

31 S. Chowdhury, J. Sikder, T. Mandal, *et al.*, Comprehensive analysis on sorptive uptake of enrofloxacin by activated carbon derived from industrial paper sludge, *Sci. Total Environ.*, 2019, **665**, 438–452.

32 X. Y. Guo, B. Du, Q. Wei, *et al.*, Synthesis of amino functionalized magnetic graphenes composite material and its application to remove Cr(VI), Pb(II), Hg(II), Cd(II) and Ni(II) from contaminated water, *J. Hazard. Mater.*, 2014, **278**, 211–220.

33 Y. Wang, W. N. Zhao, W. L. Zheng, *et al.*, Preparation of N-doped carbon nanosheets from sewage sludge for adsorption studies of Cr(VI) from aqueous solution, *Nanomaterials*, 2019, **9**(2), 265.

34 M. Naushad, T. Ahamad, B. M. Al-Maswari, *et al.*, Nickel ferrite bearing nitrogen-doped mesoporous carbon as efficient adsorbent for the removal of highly toxic metal ion from aqueous medium, *Chem. Eng. J.*, 2017, **330**, 1351–1360.

35 X. H. Thi, E. Roseline, D. Martin, *et al.*, Nitrogen-doped graphitized carbon electrodes for biorefractory pollutant removal, *J. Phys. Chem. C*, 2017, **128**(21), 15188–15197.

36 Z. G. Liu, F. Zhang, T. T. Liu, *et al.*, Removal of azo dye by a highly graphitized and heteroatom doped carbon derived fromfish waste: Adsorption equilibrium and kinetics, *J. Environ. Manage.*, 2016, **182**, 446–454.

37 J. Lin and Y. Zhan, Adsorption of humic acid from aqueous solution onto unmodified and surfactant-modified chitosan/zeolite composites, *Chem. Eng. J.*, 2012, **200**, 202–213.

38 J. Huang, W. Wu, R. Zhang, G. Lu, B. Chen, Z. Chen and C. Gui, Novel electrode material using electroless nickel plating for triboelectric nanogenerator: Study of the relationship between electrostatic-charge density and strain in dielectric material, *Nano Energy*, 2022, **92**, 106734.

39 H. P. Nogueira, S. H. Toma, A. T. Silveira, *et al.*, Efficient Cr(VI) removal from wastewater by activated carbon superparamagnetic composites, *Microchem. J.*, 2019, **149**, 104025.

40 X. Dong, L. Q. Ma, Y. Zhu, *et al.*, Mechanistic investigation of mercury sorption by Brazilian pepper biochars of different pyrolytic temperatures based on X-ray photoelectron spectroscopy and flow calorimetry, *Environ. Sci. Technol.*, 2013, **47**, 12156–12164.

41 L. Zhou, Y. G. Liu, S. B. Liu, *et al.*, Investigation of the adsorption-reduction mechanisms of hexavalent chromium by ramie biochars of different pyrolytic temperatures, *Bioresour. Technol.*, 2016, **218**, 351–359.

42 L. Dabek, Sorption of zinc ions from aqueous solutions on regenerated activated carbons, *J. Hazard. Mater.*, 2003, **101**(2), 191–201.

43 E. Dàna and A. Awad, Regeneration of spent activated carbon obtained from home filtration system and applying it for heavy metals adsorption, *J. Environ. Chem. Eng.*, 2017, **5**(4), 3091–3099.

44 S. Lata, P. K. Singh and S. R. Samadder, Regeneration of adsorbents and recovery of heavy metals: a review, *Int. J. Environ. Sci. Technol.*, 2015, **12**(4), 1461–1478.